Research Article

Dual Boundary Element Method Applied to Antiplane Crack Problems

Wei-Liang Wu

Department of Mathematics & Computer Science Education, Taipei Municipal University of Education, Taipei 10048, Taiwan

Correspondence should be addressed to Wei-Liang Wu, ozweiliang@tmue.edu.tw

This paper is concerned with an efficient dual boundary element method for 2d crack problems under antiplane shear loading. The dual equations are the displacement and the traction boundary integral equations. When the displacement equation is applied on the outer boundary and the traction equation on one of the crack surfaces, general crack problems with anti-plane shear loading can be solved with a single region formulation. The outer boundary is discretised with continuous quadratic elements; however, only one of the crack surfaces needs to be discretised with discontinuous quadratic elements. Highly accurate results are obtained, when the stress intensity factor is evaluated with the discontinuous quarter point element method. Numerical examples are provided to demonstrate the accuracy and efficiency of the present formulation.

1. Introduction

The problem of a cracked body subjected to an antiplane shear loading had been studied extensively. Sih [1] provided analytical solutions for mode III cracks in infinite regions by using Westergaard stress functions and Muskhelishvili's method. Chiang [2] presented analytical solutions for slightly curved cracks in antiplane strain in infinite regions using perturbation procedures similar to those carried out for in-plane loading cases by Cotterell and Rice [3]. Zhang [4, 5] and Ma and Zhang [6] gave analytical solutions for a mode III stress intensity factor considering a finite region with an eccentric straight crack. Ma [7] provided analytical solutions for mode III straight cracks in finite regions using Fourier transforms and Fourier series. Smith [8] studied the elastic stress distribution in the immediate vicinity of a blunt notch. However, their solutions were concerned with specified geometries or boundary conditions. To deal with the complexities of general geometries and boundary conditions, an accurate and efficient numerical method is essential [9–12].

Several numerical solutions had been devised for antiplane crack problems. Wallentin et al. [13] investigated the railway wheel crack problem numerically, based on Betti's reciprocity theorem. Guagliano and Vergani [14] described the experimental and numerical analysis of internal cracks in wheels under Hertzian loads. Paulino et al. [15] provided numerical solutions for a curved crack subjected to an antiplane shear loading in finite regions by using the boundary integral equation method. Ting et al. [16] provided numerical solutions for mode III crack problems by using the boundary element alternating method. Liu and Altiero [17] provided numerical solutions for mode III crack problems using the boundary integral equation with linear approximation on displacements and stresses. Barlow and Chandra [18] discussed the computational fatigue crack growth rate by using the crack opening displacement approach to calculate the stress intensity factors. Mews and Kuhn [19] provided numerical solutions for the traction free central crack problem by using Green's function, instead of the usual fundamental solution. Mir-Mohamad-Sadegh and Altiero [20] used the indirect boundary integral equation method to solve traction problems, using displacement-based formulations. Sun et al. [21] derived a new boundary integral equation to analyse cracked anisotropic bodies under antiplane shear. Also, for the further study, the crack front plastic deformation in a ductile material was introduced to apply the effective Dugdale strip yield model [22–24]. In general, the boundary element method (BEM) is a well-established numerical technique for the analysis of linear fracture mechanics problems. However, the solution of general crack problems cannot be achieved with the direct application of the BEM, because the coincidence of the crack surfaces gives rise to a singular system of algebraic equations.

To overcome this shortcoming, we provide an efficient numerical procedure, based on the dual boundary element method (DBEM), for antiplane shear loading problems. The dual boundary element method seems to have certain apparent advantages for in-plane loading problems with a single region formulation. This method incorporates two independent boundary integral equations, the displacement and traction equations. Portela et al. [25] considered the effective numerical implementation of the two-dimensional DBEM for solving general in-plane fracture mechanics problems. W. H. Chen and T. C. Chen [26] proposed a different DBEM formulation for in-plane crack problems. Chen and Chen suggested the use of the displacement integral equation applied only on the outer boundary and the traction integral equation on one of the crack surfaces. In Chen and Chen's formulation, relative displacement of crack surfaces was used instead of the displacement. This reduces the degrees of freedom and hence the computational effort. This study uses an integral equation formulation that combines with the crack modelling strategy of quadratic boundary elements for antiplane crack problems. The stress intensity factor is calculated based on the near tip displacement method. More accurate results are obtained by placing discontinuous quarter point elements at crack tips [27], which correctly model the behaviour of the crack tip displacement. This is a similar technique to that used for continuous quarter point elements [28]. Numerical examples are provided to demonstrate the accuracy and efficiency of the present formulation.

2. The Dual Boundary Integral Equation for Antiplane Problems

Consider a finite domain subjected to an arbitrary antiplane shear loading, where the only nonzero displacement component u_z in the z direction may be specified as follows [7]:

$$\nabla^2 u_z = 0. \tag{2.1}$$

The Laplace equation (2.1) can be transformed into a boundary integral equation, as is typical with the BEM. The boundary integral formulation of the displacement component, u_z, at an internal point $\mathbf{I}$, is given by [29]

$$u_z(\mathbf{I}) + \int_\Gamma H(\mathbf{I}, \mathbf{x}) u_z(\mathbf{x}) d\Gamma(\mathbf{x}) = \int_\Gamma G(\mathbf{I}, \mathbf{x}) t_z(\mathbf{x}) d\Gamma(\mathbf{x}), \tag{2.2}$$

where t_z represents the traction component at a boundary point $\mathbf{x}$. $H(\mathbf{I}, \mathbf{x})$ and $G(\mathbf{I}, \mathbf{x})$ represent the fundamental traction and displacement solutions, respectively, which are given as

$$H(\mathbf{I}, \mathbf{x}) = -\frac{1}{2\pi r} \frac{\partial r}{\partial \mathbf{n}}, \qquad G(\mathbf{I}, \mathbf{x}) = \frac{1}{2\pi \mu} \ln\left(\frac{1}{r}\right), \tag{2.3}$$

where μ is the shear modulus, r is the distance between $\mathbf{I}$ and $\mathbf{x}$, and $\mathbf{n}$ denotes the outward normal unit vector at the point $\mathbf{x}$ on the boundary Γ. If we consider a finite body with L cracks, (2.2) can be written as

$$u_z(\mathbf{I}) + \int_{\Gamma_S} H(\mathbf{I}, \mathbf{x}) u_z(\mathbf{x}) d\Gamma(\mathbf{x}) + \sum_{l=1}^{L} \int_{\Gamma_l^+} H(\mathbf{I}, \mathbf{x}^+) u_z(\mathbf{x}^+) d\Gamma(\mathbf{x}) + \sum_{l=1}^{L} \int_{\Gamma_l^-} H(\mathbf{I}, \mathbf{x}^-) u_z(\mathbf{x}^-) d\Gamma(\mathbf{x})$$

$$= \int_{\Gamma_S} G(\mathbf{I}, \mathbf{x}) t_z(\mathbf{x}) d\Gamma(\mathbf{x}) + \sum_{l=1}^{L} \int_{\Gamma_l^+} G(\mathbf{I}, \mathbf{x}^+) t_z(\mathbf{x}^+) d\Gamma(\mathbf{x}) + \sum_{l=1}^{L} \int_{\Gamma_l^-} G(\mathbf{I}, \mathbf{x}^-) t_z(\mathbf{x}^-) d\Gamma(\mathbf{x}), \tag{2.4}$$

where $\mathbf{x}^+$ and $\mathbf{x}^-$ are the field points located on upper and lower crack surfaces, respectively. Note that Γ_S denotes the outer boundary of the body, Γ_l^+ the lth upper crack boundary, Γ_l^- the lth lower crack boundary, and $\Gamma = \Gamma_S + \sum_{l=1}^{L}(\Gamma_l^+ + \Gamma_l^-)$. Using the fact that $H(\mathbf{I}, \mathbf{x}^+)|_{\Gamma^+} = H(\mathbf{I}, \mathbf{x}^-)|_{-\Gamma^-}$ and $G(\mathbf{I}, \mathbf{x}^+)|_{\Gamma^+} = G(\mathbf{I}, \mathbf{x}^-)|_{-\Gamma^-}$, (2.4) can be simplified to

$$u_z(\mathbf{I}) + \int_{\Gamma_S} H(\mathbf{I}, \mathbf{x}) u_z(\mathbf{x}) d\Gamma(\mathbf{x}) + \sum_{l=1}^{L} \int_{\Gamma_l^+} H(\mathbf{I}, \mathbf{x}^+) \Delta u_z(\mathbf{x}) d\Gamma(\mathbf{x})$$

$$= \int_{\Gamma_S} G(\mathbf{I}, \mathbf{x}) t_z(\mathbf{x}) d\Gamma(\mathbf{x}) + \sum_{l=1}^{L} \int_{\Gamma_l^+} G(\mathbf{I}, \mathbf{x}^+) \Delta t_z(\mathbf{x}) d\Gamma(\mathbf{x}), \tag{2.5}$$

where $\Delta u_z = u_z(\mathbf{x}^+) - u_z(\mathbf{x}^-)$ and $\Delta t_z = t_z(\mathbf{x}^+) - t_z(\mathbf{x}^-)$, however Δt_z is always zero on the crack faces. As the internal point approaches the outer boundary, that is, as $\mathbf{I} \rightarrow \mathbf{B}$, the displacement equation becomes

$$c(\mathbf{B}) u_z(\mathbf{B}) + \oint_{\Gamma_S} H(\mathbf{B}, \mathbf{x}) u_z(\mathbf{x}) d\Gamma(\mathbf{x}) + \sum_{l=1}^{L} \int_{\Gamma_l^+} H(\mathbf{B}, \mathbf{x}^+) \Delta u_z(\mathbf{x}) d\Gamma(\mathbf{x}) = \int_{\Gamma_S} G(\mathbf{B}, \mathbf{x}) t_z(\mathbf{x}) d\Gamma(\mathbf{x}), \tag{2.6}$$

where $\fint$ represents the Cauchy principle value integral and $c(\mathbf{B}) = 1/2$, given a smooth boundary at the point $\mathbf{B}$.

The stress components σ_{iz} are obtained from differentiation of equation (2.5), followed by the application of Hooke's law. At an internal point $\mathbf{I}$, these components are given by

$$\sigma_{iz}(\mathbf{I}) + \int_{\Gamma_S} S_i(\mathbf{I}, \mathbf{x}) u_z(\mathbf{x}) d\Gamma(\mathbf{x}) + \sum_{l=1}^{L} \int_{\Gamma_l^+} S_i(\mathbf{I}, \mathbf{x}) \Delta u_z(\mathbf{x}) d\Gamma(\mathbf{x}) = \int_{\Gamma_S} D_i(\mathbf{I}, \mathbf{x}) t_z(\mathbf{x}) d\Gamma(\mathbf{x}), \quad (2.7)$$

where $S_i(\mathbf{I}, \mathbf{x})$ and $D_i(\mathbf{I}, \mathbf{x})$ contain derivatives of $H(\mathbf{I}, \mathbf{x})$ and $G(\mathbf{I}, \mathbf{x})$ in the i direction, respectively, which are given as

$$S_i(\mathbf{I}, \mathbf{x}) = \frac{\mu}{2\pi r^2} \left[\frac{\partial r}{\partial x_i} \frac{\partial r}{\partial \mathbf{n}} - \left(\delta_{ij} - \frac{\partial r}{\partial x_j} \frac{\partial r}{\partial x_i} \right) n_j \right], \qquad D_i(\mathbf{I}, \mathbf{x}) = -\frac{1}{2\pi r} \frac{\partial r}{\partial x_i}, \quad (2.8)$$

where n_i denotes the ith component of the outward normal to the boundary at point $\mathbf{x}$, and δ_{ij} is the Kronecker delta. Again, by moving the source point $\mathbf{I}$ to the upper crack boundary $\mathbf{B}$, and using $t_z = \sigma_{iz} n_i$, we obtain the traction integral equation

$$\frac{1}{2} t_z(\mathbf{B}) + \int_{\Gamma_S} n_i(\mathbf{B}) S_i(\mathbf{B}, \mathbf{x}) u_z(\mathbf{x}) d\Gamma(\mathbf{x}) + \sum_{l=1}^{L} \fint_{\Gamma_l^+} n_i(\mathbf{B}) S_i(\mathbf{B}, \mathbf{x}) \Delta u_z(\mathbf{x}) d\Gamma(\mathbf{x})$$

$$= \int_{\Gamma_S} n_i(\mathbf{B}) D_i(\mathbf{B}, \mathbf{x}) t_z(\mathbf{x}) d\Gamma(\mathbf{x}), \quad (2.9)$$

where $\fint$ represents the Hadamard principal value integral. Both Cauchy and Hadamard principal-value integrals in (2.6) and (2.9) are finite parts of improper integrals. To solve the finite part integrals, we can follow the method mentioned in Portela et al. [25].

The displacement integral equation (2.6) and the traction integral equation (2.9) are the two main equations to solve for the displacement of the outer boundary and the relative displacement of the crack faces. Equation (2.6) is applied for collocation on the outer boundary where continuous quadratic elements are used, and (2.9) is applied on the upper crack faces which are modelled by discontinuous quadratic elements. By taking all the discretised nodes on the outer boundary Γ_S and upper crack surfaces $\sum_{l=1}^{L} \Gamma_l^+$ at the source point $\mathbf{B}$, the system of (2.6) and (2.9) for the multiple cracks problem can be written in a matrix form as

$$\begin{bmatrix} \mathbf{H}_1 & \mathbf{H}_2 & 0 \\ \mathbf{S}_1 & \mathbf{S}_2 & \mathbf{I} \end{bmatrix} \begin{bmatrix} \mathbf{u}_{z,S} \\ \Delta \mathbf{u}_{z,c} \\ \mathbf{t}_{z,c^+} \end{bmatrix} = \begin{bmatrix} \mathbf{G}_1 \\ \mathbf{D}_1 \end{bmatrix} [\mathbf{t}_{z,S}], \quad (2.10)$$

where $\mathbf{H}_1$, $\mathbf{H}_2$, $\mathbf{G}_1$ and $\mathbf{S}_1$, $\mathbf{S}_2$, $\mathbf{D}_1$ are the corresponding assembled matrices from (2.6) and (2.9), respectively. The $\mathbf{u}_{z,S}$ and $\mathbf{t}_{z,S}$ are the displacement and traction vectors on the outer boundary Γ_S, respectively. $\Delta \mathbf{u}_{z,c}$ and $\mathbf{t}_{z,c^+}$ are the relative displacement vector and the traction vector on the upper crack faces.

3. Calculation of the Mode III Stress Intensity Factor

Near tip displacement extrapolation is used to evaluate the numerical values of the stress intensity factor. The relative displacements of the crack surfaces are calculated using the DBEM and are used in the near crack tip stress field equations to obtain the stress intensity factor. Due to the singular behaviour of the stress around the crack tip, it is reasonable to expect a better approximation by replacing the normal discontinuous quadratic element with a transition element possessing the same order of singularity at the crack tip. The discontinuous quarter point element method is used in the present formulation [27, 30]. The mode III stress intensity factor is evaluated as

$$K_{\mathrm{III}} = \frac{\mu}{4}\sqrt{\frac{2\pi}{r}}\Delta u_z(r), \tag{3.1}$$

where r is the distance from the crack tip to the nearest node on the upper crack face, and $\Delta u_z(r)$ denotes the relative displacement in the antiplane direction.

4. Numerical Examples

In order to demonstrate the accuracy and efficiency of the technique previously described, and to illustrate possible applications, we now consider several examples. In all the numerical tests, the outer boundary is modelled by 24 continuous quadratic elements, and each crack discretization is carried out with three different meshes of 6, 8, and 10 discontinuous quadratic elements, respectively. The best accuracy is achieved with 6 elements, in which the crack discretization is graded, towards the tip, with ratios 0.25, 0.15, and 0.1. The plate is subjected to a uniform antiplane shear loading τ, and the stress intensity factor is normalised with respect to

$$K_0 = \tau\sqrt{\pi a}, \tag{4.1}$$

where a defines the half length of the crack. All computations are carried out under the condition of plane strain.

4.1. A Rectangular Plate Containing a Central Slant Crack

Firstly, consider a rectangular plate containing a central slant crack as shown in Figure 1. The crack has length $2a$ and makes an angle θ with the horizontal direction. For a horizontal crack ($\theta = 0°$), the normalised mode III stress intensity factor is calculated for various ratios of a/h and a/w and compared to those given in [17, 31] (see Table 1). The largest difference between these does not exceed 1.65 per cent. Further, the normalised mode III stress intensity factor is calculated for $h/w = 2$, while the crack slanted an angle θ with the various ratios of a/w. Three cases are considered, where $\theta = 30°$, $45°$, and $60°$, respectively. The results obtained are presented in Figure 2. As it can be seen, when the ratio of a/w increases, the stress intensity factor increases due to edge effect.

For the case where $a/w = 1/50$, which could be considered as the case of infinite geometry since $a \ll w$, we compare the results with the analytical results for the latter
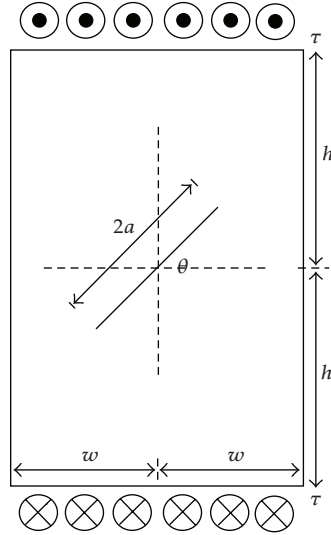
Figure 1: Rectangular plate with a central slant crack.

Table 1: Normalised mode III stress intensity factor for a straight central crack.

	$a : h$	$1 : 0.25$	$1 : 0.5$	$1 : 1$	$1 : 2$	$1 : 4$
$a : w$	Present	1.909	1.724	1.689	1.688	1.661
$1 : 1.2$	Reference [17]	1.897	1.723	1.689	1.686	1.686
	Reference [31]	1.900	1.725	1.691	1.689	1.689
$a : w$	Present	1.796	1.467	1.371	1.361	1.361
$1 : 1.4$	Reference [17]	1.780	1.460	1.369	1.359	1.358
	Reference [31]	1.782	1.463	1.370	1.361	1.360
$a : w$	Present	1.784	1.405	1.257	1.236	1.236
$1 : 1.6$	Reference [17]	1.771	1.399	1.254	1.233	1.233
	Reference [31]	1.773	1.401	1.256	1.235	1.235
$a : w$	Present	1.792	1.384	1.179	1.131	1.129
$1 : 2.0$	Reference [17]	1.770	1.377	1.176	1.127	1.126
	Reference [31]	1.772	1.379	1.178	1.130	1.128

as given in [32]. The results are plotted in Figure 3. Excellent agreement is observed; the maximum error is around 0.02 per cent.

4.2. A Rectangular Plate Containing Two Identical Collinear Cracks

As shown in Figure 4, the second example is a rectangular plate containing two identical collinear cracks. $2a$ is the length of the inclined crack and $2d$ is the distance between the centre of the cracks. The geometric parameters are $h/w = 2$ and $a/w = 1/50$. Figure 4 displays the variations of normalised mode III stress intensity factors at tip A and tip B versus different ratios of a/d. Due to the interaction between the two cracks, the computed normalised mode III stress intensity factor at tip A is always larger than that at tip B. Hence, as the crack centre distance d decreases, the difference of stress intensity factor increases. There is excellent
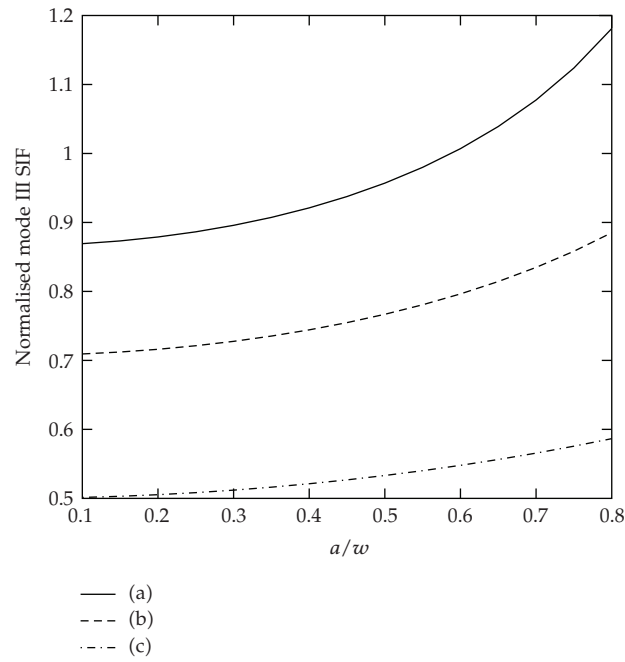
Figure 2: The rectangular plate with a central slant crack at (a) $\theta = 30°$, (b) $\theta = 45°$, and (c) $\theta = 60°$.
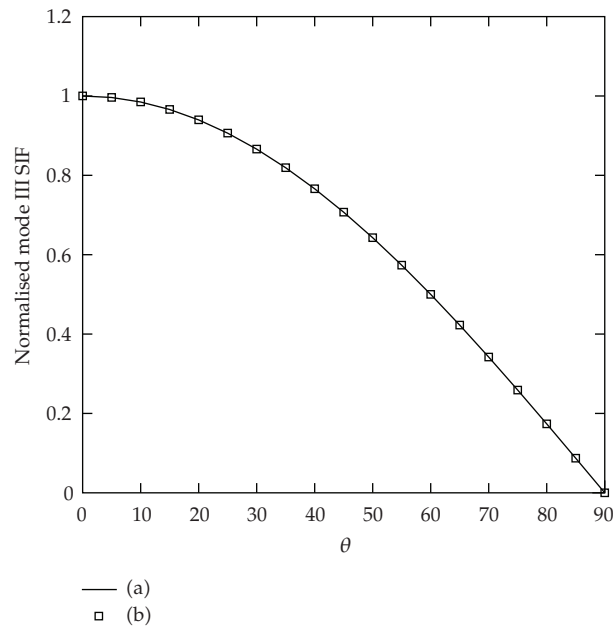

Figure 3: The infinite plate with a central slant crack: (a) the analytical solutions and (b) the present method.
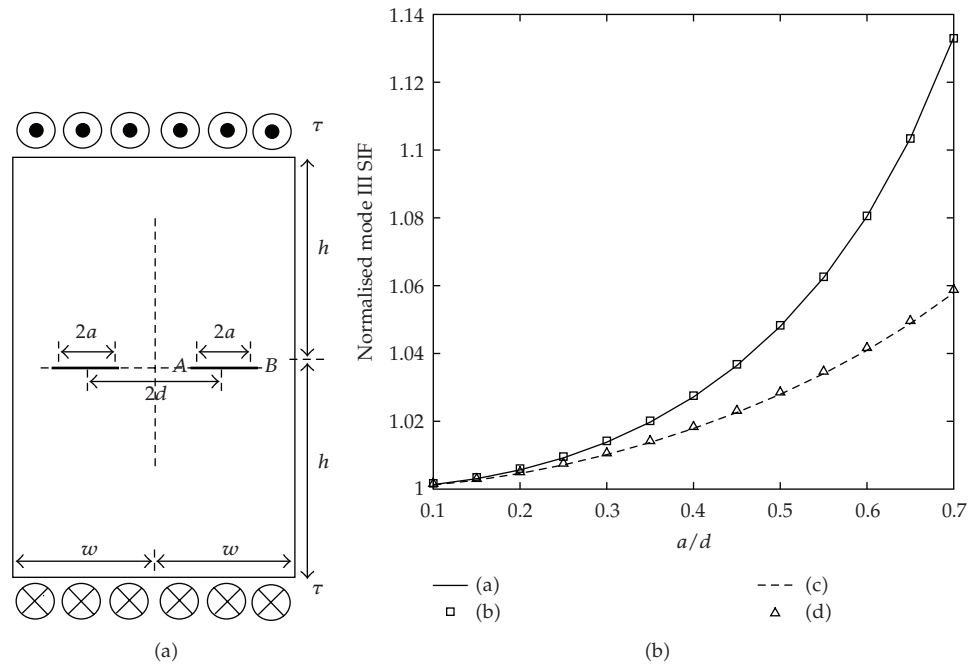
Figure 4: The rectangular plate with two identical collinear cracks. Normalised mode III stress intensity factors versus a/d for tip A: (a) the analytical results and (b) the present method, and for tip B: (c) the analytical solutions and (d) the present method.
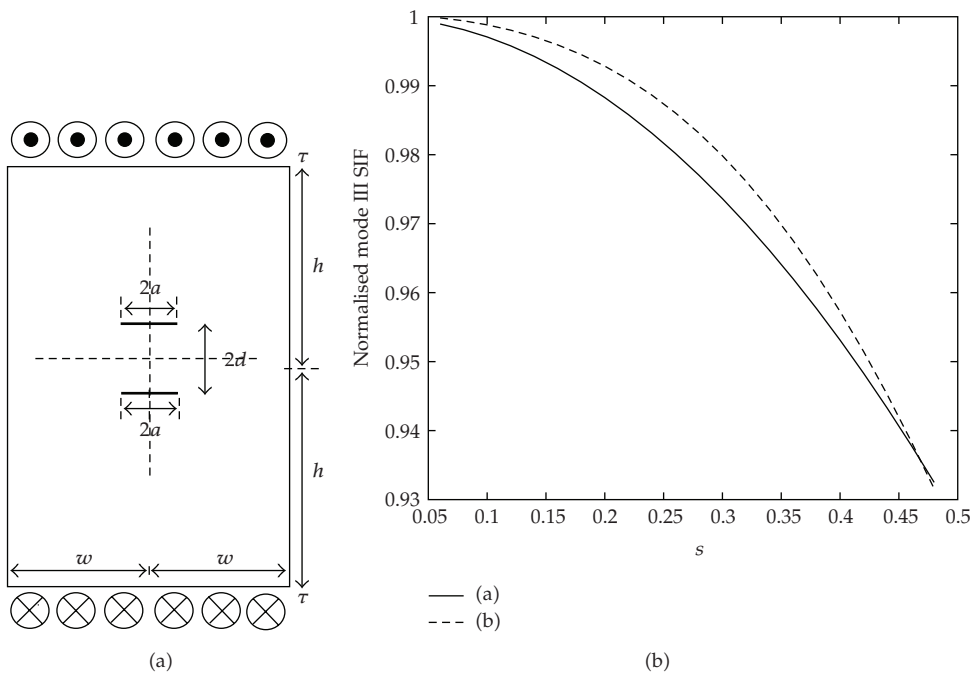

Figure 5: The rectangular plate with two parallel cracks. Normalised mode III stress intensity factors versus s for (a) [32] and (b) the present method.

correlation between the computed results using the present method and those from analytical solutions; the difference between these results does not exceed 0.03 per cent at tip *A* or 0.09 per cent at tip *B*.

4.3. An Infinite Plate Containing Two Parallel Cracks

The third example is an infinite plate ($h/w = 2$, $a/w = 1/50$) containing two parallel cracks, as shown in Figure 5. $2a$ is the length of the two identical cracks and $2d$ is the distance between the cracks. The computed results are compared with the published results in [32]. The results of normalised mode III stress intensity factor for different s are plotted in Figure 5, where $s = a/(a + d)$. The effect of the interaction of cracks on the mode III stress intensity factor is observed. The largest difference between the present and the published results does not exceed 0.65 per cent.

5. Conclusions

An efficient and accurate dual boundary element technique has been successfully developed for the analysis of two dimensional cracks subjected to an antiplane shear loading. The dual boundary equations are the usual displacement boundary integral equation and the traction boundary integral equation. When the displacement equation is applied on the outer boundary and the traction equation is applied on one of the crack surfaces, a general crack problem can be solved in a single region formulation. The discontinuous quarter point elements are used for evaluating the mode III stress intensity factor, which correctly describes the $r^{1/2}$ behaviour of the near tip displacements. This, therefore, allows accurate results for mode III stress intensity factors to be calculated.

References

[1] G. C. Sih, "Stress distribution near internal crack tips for longitudinal shear problems," *Journal of Applied Mechanics*, vol. 32, pp. 51–58, 1965.

[2] C. R. Chiang, "Slightly curved cracks in antiplane strain," *International Journal of Fracture*, vol. 32, no. 4, pp. R63–R66, 1986.

[3] B. Cotterell and J. R. Rice, "Slightly curved or kinked cracks," *International Journal of Fracture*, vol. 16, pp. 155–169, 1980.

[4] X. S. Zhang, "The general solution of a central crack off the center line of a rectangular sheet for mode III," *Engineering Fracture Mechanics*, vol. 28, no. 2, pp. 147–155, 1987.

[5] X. S. Zhang, "A tearing mode crack located anywhere in a finite rectangular sheet," *Engineering Fracture Mechanics*, vol. 33, no. 4, pp. 509–516, 1989.

[6] S. W. Ma and L. X. Zhang, "A new solution of an eccentric crack off the center line of a rectangular sheet for mode-III," *Engineering Fracture Mechanics*, vol. 40, no. 1, pp. 1–7, 1991.

[7] S. W. Ma, "A central crack of mode III in a rectangular sheet with fixed edges," *International Journal of Fracture*, vol. 39, no. 4, pp. 323–329, 1989.

[8] E. Smith, "A comparison of Mode I and Mode III results for the elastic stress distribution in the immediate vicinity of a blunt notch," *International Journal of Engineering Science*, vol. 42, no. 5-6, pp. 473–481, 2004.

[9] P. H. Geubelle and M. S. Breitenfeld, "Numerical analysis of dynamic debonding under anti-plane shear loading," *International Journal of Fracture*, vol. 85, no. 3, pp. 265–282, 1997.

[10] E. Heymsfield, "Infinite domain correction for anti-plane shear waves in a two-dimensional boundary element analysis," *International Journal for Numerical Methods in Engineering*, vol. 40, no. 5, pp. 953–964, 1997.

[11] S. M. Mkhitaryan, N. Melkoumian, and B. B. Lin, "Stress-strain state of a cracked elastic wedge under anti-plane deformation with mixed boundary conditions on its faces," *International Journal of Fracture*, vol. 108, no. 4, pp. 291–315, 2001.

[12] Z.-G. Zhou and L. Ma, "Two collinear Griffith cracks subjected to anti-plane shear in infinitely long strip," *Mechanics Research Communications*, vol. 26, no. 4, pp. 437–444, 1999.

[13] M. Wallentin, H. L. Bjarnehed, and R. Lundén, "Cracks around railway wheel flats exposed to rolling contact loads and residual stresses," *Wear*, vol. 258, no. 7-8, pp. 1319–1329, 2005.

[14] M. Guagliano and L. Vergani, "Experimental and numerical analysis of sub-surface cracks in railway wheels," *Engineering Fracture Mechanics*, vol. 72, no. 2, pp. 255–269, 2005.

[15] G. H. Paulino, M. T. A. Saif, and S. Mukherjee, "A finite elastic body with a curved crack loaded in anti-plane shear," *International Journal of Solids and Structures*, vol. 30, no. 8, pp. 1015–1037, 1993.

[16] K. Ting, K.-K. Chang, and M.-F. Yang, "Analysis of mode III crack problems by boundary element alternating method," in *Fatigue, Flaw Evaluation and Leak-Before-Break Assessments*, vol. 280, pp. 21–26, American Society of Mechanical Engineers, 1994.

[17] N. Liu and N. J. Altiero, "An integral equation bethod applied to mode III crack problems," *Engineering Fracture Mechanics*, vol. 41, pp. 578–596, 1992.

[18] K. W. Barlow and R. Chandra, "Fatigue crack propagation simulation in an aircraft engine fan blade attachment," *International Journal of Fatigue*, vol. 27, no. 10–12, pp. 1661–1668, 2005.

[19] H. Mews and G. Kuhn, "An effective numerical stress intensity factor calculation with no crack discretization," *International Journal of Fracture*, vol. 38, no. 1, pp. 61–76, 1988.

[20] A. Mir-Mohamad-Sadegh and N. J. Altiero, "Solution of the problem of a crack in a finite plane region using an indirect boundary-integral method," *Engineering Fracture Mechanics*, vol. 11, no. 4, pp. 831–837, 1979.

[21] Y.-Z. Sun, S.-S. Yang, and Y.-B. Wang, "A new formulation of boundary element method for cracked anisotropic bodies under anti-plane shear," *Computer Methods in Applied Mechanics and Engineering*, vol. 192, no. 22-23, pp. 2633–2648, 2003.

[22] J. Vrbik, B. M. Singh, J. Rokne, and R. S. Dhaliwal, "Plastica deformation at the tip of an edge crack," *Zeitschrift für Angewandte Mathematick und Mechanik*, vol. 81, pp. 642–647, 2001.

[23] H. T. Danyluk, B. M. Singh, and J. Vrbik, "Plastic zones in an orthotropic plate of finite width containing a Griffith crack," *International Journal of Fracture*, vol. 75, no. 4, pp. 307–322, 1996.

[24] X. Jin, S. Chaiyat, L. M. Keer, and K. Kiattikomol, "Refined Dugdale plastic zones of an external circular crack," *Journal of the Mechanics and Physics of Solids*, vol. 56, no. 4, pp. 1127–1146, 2008.

[25] A. Portela, M. H. Aliabadi, and D. P. Rooke, "The dual boundary element method: effective implementation for crack problems," *International Journal for Numerical Methods in Engineering*, vol. 33, no. 6, pp. 1269–1287, 1992.

[26] W. H. Chen and T. C. Chen, "An efficient dual boundary element technique for a two-dimensional fracture problem with multiple cracks," *International Journal for Numerical Methods in Engineering*, vol. 38, pp. 1739–1756, 1995.

[27] A. Saez, R. Gallego, and J. Dominguez, "Hypersingular quarter-point boundary elements for crack problems," *International Journal for Numerical Methods in Engineering*, vol. 38, pp. 1681–1701, 1995.

[28] J. Martinez and J. Dominguez, "On the use of quarter-point boundary elements for stress intensity factor computations," *International Journal for Numerical Methods in Engineering*, vol. 20, no. 10, pp. 1941–1950, 1984.

[29] C. A. Brebbia and J. Dominguez, *Boundary Elements: An Introductory Course*, Computational Mechanics, Southampton, UK, 1989.

[30] P. Fedelinski, M. H. Aliabadi, and D. P. Rooke, "A single-region time domain BEM for dynamic crack problems," *International Journal of Solids and Structures*, vol. 32, no. 24, pp. 3555–3571, 1995.

[31] S. W. Ma, "A central crack in a rectangular sheet where its boundary is subjected to an arbitrary anti-plane load," *Engineering Fracture Mechanics*, vol. 30, no. 4, pp. 435–443, 1988.

[32] H. Tada, P. Paris, and G. Irwin, *The Stress Analysis of Cracks Handbook*, Paris Productions Incorporated, St. Louis, Mo, USA, 1985.